Al-Rafidain Engineering Journal (AREJ) Vol.28, No.1, March 2023, pp. 280-292

The Experimental Impact of Convective Heat Transfer Improvement from Numerous Perforated Shape Fin Array

Noori Raad Noori* noorikhlka34@gmail.com

Arkan Fawzi Saeed** arkan.alhazeen@uod.ac

* Power Engineering Department, University of Polytechnic-Duhok, Duhok, Iraq
** Mechanical Engineering Department, College of Engineering, University of Duhok, Duhok, Iraq

Received: 2022-10-19 Received in revised form: 2022-11-22 Accepted: 2022-12-4

ABSTRACT

The current work explores a trial forced convective heat move from rectangular blades on an upward surface at low Reynolds numbers. The heat removal for a proper number of punctured and non-punctured fins, fin dividing, and length was estimated in an upward air stream for fluctuating inlet air speed and some way or another low info heat power somewhere in the range of 20W and 70W. The characteristics are investigated for rectangular, circular, and V-shape perforated fin array against non-perforated one. The impact of different boundaries, like heat input with various liquid stream speed on average coefficient of heat transfer (h) improvement has been considered. The impact of the Nusselt numberand Reynolds number, were practically examined. The heat loss has been improved by increasing the heat transfer coefficient between the fin total surface and its encompassing, through increasing the area of heat to remove all out surface through fin perforations. The trial relations have been differentiated by correlating Nu and Re for non-punctured plate heat sink, the reach $6*10^3 \leq Re \leq 19*10^3$, and $Pr \cong 0.7$ with error ±7%, and punctured finned plate heat sink with the reach $6*10^3 \leq Re \leq 20*10^3$, and $Pr \cong 0.7$ with a deviation factor $R^2=0.995$.

Keywords:

Forced convection. Heat transfer enhancement. Perforated Fin.

https://rengj.mosuljournals.com

1. INTRODUCTION:

In numerous modern industrial frameworks, heat should be moved either to enter energy into the framework or to ask block the energy processed inside the framework. Taking into account the quick expansion in energy request around the world, both decreasing energy lost because of inadequate use and improvement of the energy transfer inside the appearance of heat turned into an undeniably significant errand for the look and action engineers of such frameworks [1].

Akyol and Bilen [2]have performed a trial investigation on the heat transfer and friction head loss coefficient through perforated rectangular profile fins surfaces with a Reynolds number ranging from $(3 \times 10^3 - 32 \times 10^3)$ that is primly based on an average inlet velocity and hydraulic diameter. Fins were placed perpendicularly to the heating surface. The perforated rectangular fins with both the inline and staggered fin patterns have been investigated with four varied stream wise and one constant span wise. The correlation equations of Nusselt and friction factor and heat transfer efficiency have been specified for the fin case and no fin case. The result has shown that both the fin patterns have considerably increased the heat transferred through the fin compared with no fin case. Also, another indication has been observed that the Nusselt number is proportional to the Reynolds number with both the projected area and total surface area including both fin patterns (Inline and staggered). They attained more enhanced heat transfer for the staggered fin pattern with total surface area as a result of the turbulent flow and better flow mixing. Because of the staggered pattern, increasing the Reynolds number has resulted in an increase in pressure drop and friction factor due to the occlusion effect created in the fluid flow.

Kavita, H. D. et.al, [3], the researchers had conducted an experimental study on heat transfer improvement through vertical rectangular fin arrays with circular perforations. The experimental analysis was taken for aluminum material at 200 W heat input and a varied Reynolds number from $(2.1 \times 10^4 - 8.7 \times 10^4)$

and different sizes of the perforations and fin thickness. The Nu number was taken as average in the experiment. The design parameters have been investigated by using an experimental design approach which is called Taguchi. Also, the best possible results have been determined experimentally by using porosity. The results had shown that by increasing porosity and the Re number to the maximum value used in the experiment, a considerable effect on Nu was noticed. It was shown from the experimental approach method that Re number was found to have the most impact on heat transfer performance, followed by porosity and then fin thickness, according to the experimental approach method. The optimum heat transfer performance was obtained at 8.7×10^4 Re, 5mm thickness of fin, 0.22 porosity. Another conclusion shown by the result which indicated that the Nu number had increased for both fin models when increasing the Re number and also Nu number for the perforated fin was more than the finned one due to the extra heat sink created by the perforations which have allowed a more free movement of air and more turbulent vortexes. On the other hand, fin effectiveness was optimum for the perforated fin at the same Re number, especially at a high porosity of 0.22. Increasing porosity caused the friction factor to increase.

Ibrahim T. K., et.al, [4], had performed an investigation on heat transfer within perforated rectangular shape fins by changing the perforation shape and their geometry. A heat exchanger was used with the perforated fins under forced convection. Several fin perforations were used in the experiment which are rectangular, circular and triangular, and non-perforated fins. The result had showed that by using fin perforations, a higher temperature difference had been achieved than the non-perforated one. Also, more heat transfer coefficient had been achieved which is about 35.82 to 51.29 percent regardless of the fin shape and geometry. The result had showed that the circular perforations had the highest temperature difference comparability to the temperature at the fin tip with the heat collector temperature, rectangular perforation comes in second place and triangular in third place.

Mahathir Mohammad, et.al, [5], had investigated the effect of varying the geometry and perforation shape of the rectangular fins to find the best perforation shape that leads to a significant elevation in the performance of heat transfer and effectiveness. The result had showed that the temperature distribution for the punctured fin had a greater drop in temperature than the non-perforation fins. Another indication had been noticed that the fin with triangular perforation under 150 W heat input had a raise in the coefficient of heat transfer by 78.98% more than the non-perforated fins and the other perforations (rectangular and circular) had a 74.4 % and 41.4 % increase than the non-perforated fins respectively. Also, triangular fin perforation had the highest temperature distribution under 100 W of heat input with a percent of 54.5 %, and 38 %, 33.04 % for rectangular and circular respectively. The result showed that triangular perforation had a 25.7 % higher temperature difference than the non-perforated one which had a percentage of 18.84 %.

Adhikari R. C. et.al, [6], had conducted an experimental with a numerical study on heat transfer through rectangular fins under low Re numbers that range from 2600 to 6800. The experimental study was made through a wind tunnel with an array of rectangular fins under different air speeds and other factors (including Re and h). The results showed that there was a 4.281 percent of error between the practical and numerical for the heat transfer coefficient and Nu number. An indication was found by the experimental procedures which indicates that the relation between Nu and Re numbers was almost linear for turbulent fully developed flow and well-distributed heat flux. A numerical study was conducted for the different fin geometries. It was found that by increasing the channel length, the heat transfer tends to decrease linearly with the channel length. On the other hand, it stays constant with the increasing number of fins.

Ibrahim T. K. et.al, [7], has conducted an experimental and numerical study on the effect of using rectangular fins with square perforations on heat transfer. The experiments were done under heat input rates of 1730, 2200, 2680 and, 3150 W and air speeds of 0.4, 0.7, 1.1, 1.4 and, 1.8 m/s.

After the result had been found in the experimental and numerical procedures, less percent of error was contributed. The result had showed that the temperature distribution across the perforated fins had a 16 ^{o}C Temperature reduction than the one with non-perforations.

Also, by grooving more perforations to the rectangular fins, more heat transfer rates had been achieved as a result of turbulent flow created through the perforations and the decreased level of thermal resistance. Another indication had been achieved by using perforated fins that the friction factor had been reduced which in turn had saved some energy from being lost by the pumping power. Finally, by using the rectangular fins with a square perforation model, a 5.91 %

drop in friction factor had been achieved compared with circular perforation.

Kaladgi A. R. et.al, [8], had conducted a numerical study on the effect of using rectangular fins with extended circular perforations on heat transfer performance. Their work identifies the temperature distribution across a variety of circular perforations. The numerical analysis was done under the professional program which is used widely and it's called (ANSYS FLUENT Software). The result had showed that by using the specified model mentioned above, an effective temperature decrease across the fin was achieved, and enhanced heat transfer performance was observed.

In the present work, the experiments were conducted in three-dimensional steady-state, forced-convection heat transfer in a turbulent region, with rectangular fin arrays heated with a constant power input from 20 - 70 W step 10W, in a range of Reynolds number ($6200 \leq Re \leq 18700$) and Pr = 0.71. Rectangular fins manufactured from yellow Brass, solid flat plate, and flat plate with various perforations, Rectangular (Inline pattern), Circular (Inline pattern), and V-shape (Inline pattern). A total of 24 fins models were designed by AutoCAD and manufactured by CNC machine. The effect of various perforation shapes on heat transfer performance has been studied for each power input with various Reynolds number, taking into consideration the effect of reduction area (RAF) on the heat transfer coefficient.

2. EXPERIMENTAL APPARATUS

2.1. Main unit:

The fundamental unit is a smaller seat mounting outline that interfaces with a reasonable electrical stockpile. It has an upward conduit gathering and a primary 'Control Board' with computerized show as displayed in Figure (1).

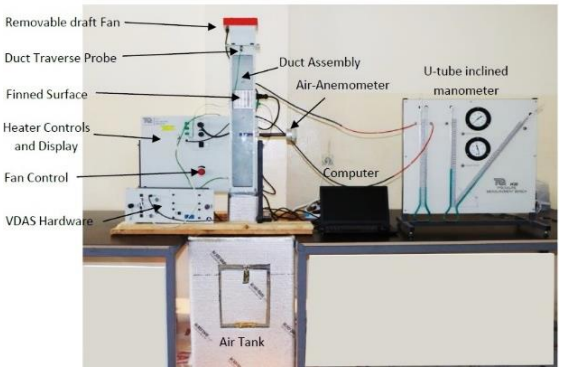

Figure (1): Free and Forced convection TD1005 with VDAS data acquisition system.

And the apparatus particulars recorded in Table (1).

Item	Details
Operating Environment	Indoor (laboratory) Altitude up to 2000 m Temperature range 5°C to 40°C Maximum relative humidity 80% for temperatures up to 31°C, decreasing linearly to 50% relative humidity at 40°C Overvoltage category 2 (as specified in EN61010-1). Pollution degree 2 (as specified in EN61010-1).
Nett Dimensions (assembled)	550 mm front to back, 850 mm wide and 1200 mm high
Nett Weight (assembled)	Main unit: 26 kg (with no heat transfer surface fitted)
Electrical Supply	Single phase 50 Hz to 60 Hz 100 VAC to 120 VAC at 1.2 A or 220 VAC to 240 VAC at 0.6 A Specified on order
Fuse	20 mm 6.3 A Ceramic Type F
External connections	Heater, air velocity sensor, thermocouple and VDAS sockets - Extra Low Voltage (<25 VDC) Fan socket (rear of equipment) - 0 VAC to mains supply voltage.
Thermocouple inputs	3 off type K Displayed resolution 0.1°C
Heater output and display	Maximum power approximately 100 W Displayed resolution 0.1 W
Duct	Nominal internal cross section: 128 mm x 75 mm = 0.0096 m^2 Approximate length: 850 mm Nominal air velocity: Greater than 3.8 $m.s^{-1}$ with flat plate. Normal experiment velocity: 3.5 $m.s^{-1}$or less. Probe positions (away from heat transfer surface): 7.5 mm, 19.5 mm, 31.5 mm, 43.5 mm, 55.5 mm and 67.5 mm
Anemometer Range	0 to 3.8 $m.s^{-1}$

Table (1): Specifications of the main unit.

Heat transfer surfaces are fitted just right above halfway of the back side of the vertical wind tunnel. The air flows over the heat transfer surfaces by forced convection with the use of an induced updraft fan which is located exactly at the top of the wind tunnel. A calibrated thermocouple has been used to measure the inlet air temperature that has been fixed carefully at the inlet of the wind tunnel. Another calibrated portable thermocouple probe in a traversing mechanism is also placed carefully at the outlet of the duct in the middle position. The flow velocity is measured by a calibrated anemometer placed below the test section, and the surface temperature of the fin base is measured by a built-in K-type thermocouple. Also, another hand-held K-type calibrated thermocouple has been used for measuring the temperature distribution along the fin. The hand-held thermocouple probe was inserted into six equally spaced holes which have been placed on the side facade of the duct in addition to the magnetic wrapper that allows the holes to be wrapped entirely and measureseach temperature individually and accurately by reducing the stray convection caused by the other holes. The electrical power is supplied safely to the heater in each heat transfer surface and to the fan which is placed at the top of the duct. The heat transfer surface is widely used as heat sink that conducts the heat away from electrical components and electrical circuits as shown in Figure (2), where six equally distributed holes were placed in the side of the duct which is exactly near the side of the fins in order to measure the temperature distribution across the fin.

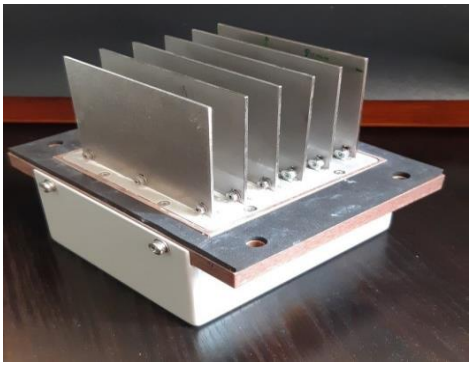

Figure (2): Finned Surface.

The heat transfer surface is widely popular because of the extra heat sink provided by fin perforations. This heat sink helps in dissipating more heat from the base plate to air which helps in better cooling and at the same time helps in saving fin material and cost. Also, this improved heat sink can have many adjustments to obtain a better performance such as changing the shape of perforations, number, size, etc. The perforated finned surfaces used presently are exhibited in Figure (3).

Figure (3): Specimen Perforated Finned Surface.

Table (2): Heat Transfer surfaces technical details.

Experiments	Details
Flat plate	Plate material: 3mm thickness of aluminum Total surface area: *106*mm**106*mm K-type thermocouple on the back side of the flat plate Net dimensions:*160*mm**140*mm**125*mm and 1227 g
Finned surface	Which includes flat plate and 6 fins placed perpendicular to the flat plate. Fin dimensions: 90mm*73mm*1.5mm. Total surface area: 0.092 m^2 (with fin tip) as shown in fig (2).
Perforated Finned Surface	Fin dimensions: 90 mm x 73mm x 1.5 mm. Perforation shape: Rectangular, Circular and V-shape inline patterns, as shown in fig (3).

An Air-tank features one hole in both sides and a door equipped with a lock, provided with insulation for controlling the heat up or cooling down the container air temperature depending on weather conditions. Heating or cooling the air in winter or summer requires a special control within the container to raise or lower the temperature a few degrees.

2.2. Temperature measurement:

For measuring temperature, several calibrated thermocouples of the type-K were utilized to quantify the temperature of the inlet and outlet air stream with the finned array base. These thermocouples were connected to the selector switch by type-K connection wire, then to the digital display of the main unit which has a display error of 0.1 ºC. Also, a hand-held thermocouple with type-K were used to measure the temperature distribution across the fins. This thermocouple is connected with a type-K wire to a digital temperature meter K-type which has a temperature range (-50 ºC- 1300 ºC), and a display error of 0.1 ºC. Figures (4) and (5) show the calibration curves of the used thermocouples.

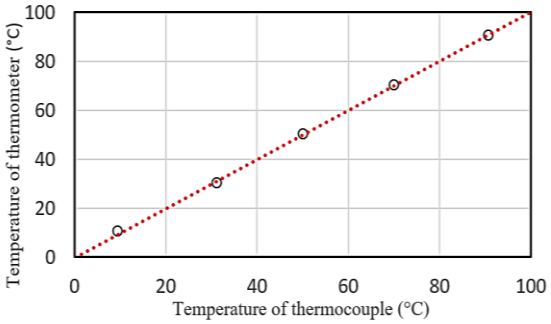

Figure (4): Calibration curve of the thermocouples.

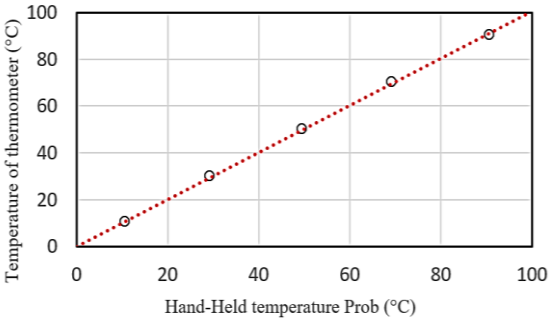

Figure (5): Calibration curve of the hand-held temperature probe.

2.3. Air velocity measuring device:

A hot wire anemometer shown previously in Figure (1) was installed inside the wind tunnel in order to measure air velocity which has a range (0m/s-3.8m/s) and error of 0.03%. VOLTCRAFT AN-10 digital anemometer handheld 0.1 up to 30 m/s Magnetic vane anemometer was used for calibrating air velocity. The calibrating curve is displayed in Figure (6).

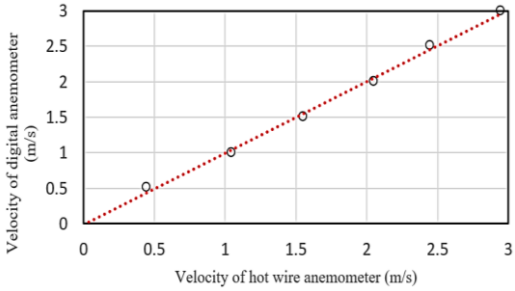

Figure (6): Calibrating curve of Air flow velocity.

The laboratory device has been allowed to operate for a period of time in order to specify the time required for the temperatures to stabilize depending on the material used in the experiments. The time taken for the temperature to stabilize is approximately (20-35) minutes. To make sure of reliability, the experiment was repeated twice. The standard deviation of numerous experiments was determined to ascertain the accuracy at each temperature position. The temperature variations between the foundations of the fins were found to be within a range of ±0.4 ºC based on the digital thermocouple measurements. The range of the thermocouples used to measure the free stream temperature was within ±0.3 ºC of the average temperature recorded at the wind tunnel's inlet. Using the data acquired from each experiment, the average air speed values, surface temperatures of the fin, and then the descent in pressure across-test the instrument were measured. Figure (7) illustrates how consistently the readings were repeated.

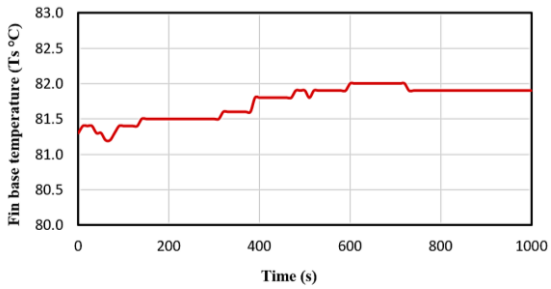

Figure (7): Brass steady state. This test is done under Q input of 70 W and velocity of 1m/s.

Figures (8-a, and b), represent the repetition reading of the temperature taken from the experiment for different input power.

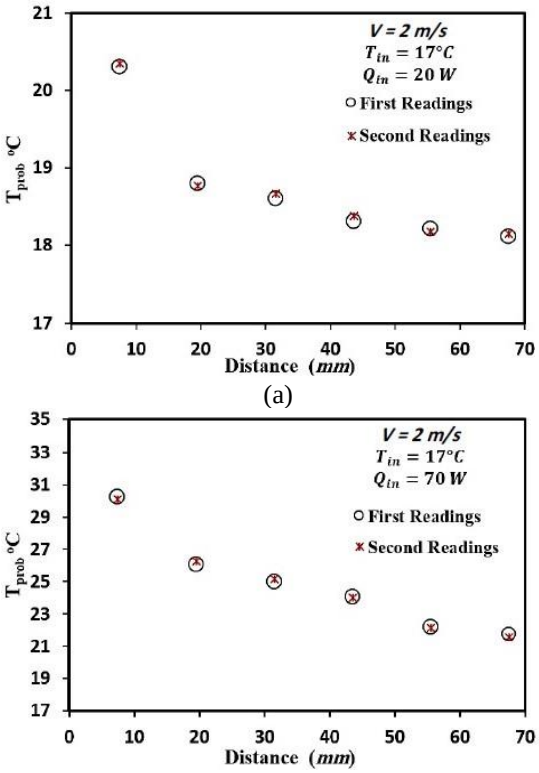

Figure (8): Reading repetitions for temperature distribution of input power: (a) 20W, (b) 70W

3. DATA PROCESSING:

3.1. working fluid's Thermo-Physical attributes:

The huge temperature variation distinction between the fluid and consequently, surface temperatures of the fin has an enormous effect on the thermo-physical characteristics of the testing fluid that is air. As a quotient, the density, thermal conductivity, dynamic viscosity, and specific heat capacity of air were thought to be temperature-dependent qualities. The following correlations were used to calculate the density, thermal conductivity, specific heat, and dynamic viscosity of air at temperatures between 273.15 and 373.15 K (0-100 ºC). [9]:

$$\rho_{air} = 362.74 * (T_f)^{-1.004} \quad (1)$$

$$k_{air} = -0.001 + 0.0001 * (T_f) - 6 * 10^{-8}(T_f)^2 + 2 * 10^{-11}(T_f)^3 \quad (2)$$

$$Cp_{air} = 1.0405 - 0.0003 * (T_f) + 6 * 10^{-7}(T_f)^2 - 3 * 10^{-10}(T_f)^3 \quad (3)$$

$$\mu_{air} = 5 * 10^{-7} + 7 * 10^{-8} * (T_f) - 5 * 10^{-11}(T_f)^2 + 2 * 10^{-14}(T_f)^3 \quad (4)$$

Where the air properties were taken at average air mean temperature (T_{avg}).

$$T_{avg} = \frac{T_{in} + T_{out}}{2} \quad (5)$$

3.2. Heat Transfer Calculation:

The power provided by the electrical supply to the heat transfer surfaces is turned into three thermal power types which can be expressed as follows: -

$$W = \dot{Q}_{cond} + \dot{Q}_{conv} + \dot{Q}_{rad} \quad (6)$$

The heat transfer loss by conduction and radiation has been minimized using insulation materials on the bare metal surfaces. This means that the power provided by the electrical power supply will equalize approximately the heat transferred by convection, which can be expressed as follows: -

$$W \approx \dot{Q}_{conv} \quad (7)$$

The maximum heat transfer conducted by one fin through convection can be given as follows:-

$$Q_{max} = h \times A_f \times T_m \quad (8)$$

Heat transfer conducted by one fin is also given as:-

$$Q_f = k \times A_c \times m \times T_m \times \tanh(m \times L_c) \quad (9)$$

$$m = \sqrt{\frac{h \times p_e}{k \times A_c}} \quad (10)$$

Where; k is the thermal conductivity of the material. In order to account for end loss of fin, L_c instead of L is used which represent the fin characteristics length. Heat transfer conducted through convection without fins can be expressed as the following equation:-

$$Q_{nf} = h \times A_b \times T_m \quad (11)$$

After obtaining the experimental readings that have been recorded by thermocouples, the LMTD has been calculated for each reading that includes the specified velocity and heat input. LMTD has been used instead of mean temperature because as time passes the heat transfer rate changes, so it is more desirable to use LMTD and can be expressed by the following equation: -

$$T_m = \frac{T_{out} - T_{in}}{ln\frac{T_s - T_{in}}{T_s - T_{out}}} \quad (12)$$

Where T_{in}, T_{out} and T_s are air inlet, outlet, and fin base surface temperatures respectively. Figures (9-a, and b) represents the LMTD reading repetition of the yellow Brass specimens under lab test.

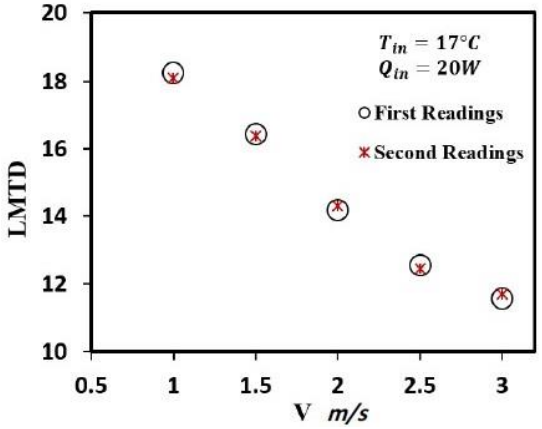

(a)

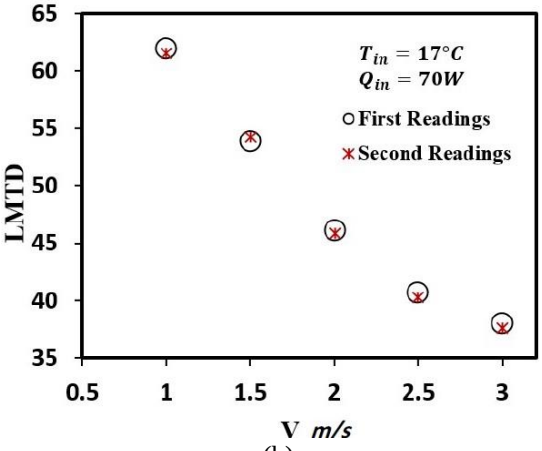

(b)

Figure (9): Reading repetitions for logarithmic mean temperature difference LMTD of input power: (a) 20W, (b) 70W.

3.3. Calculations of Specimen surface area and cross sectional area:

The surface area of fin base without fins has been derived as follows: -

$$A_b = A_v - n \times A_c \quad (13)$$

Where; A_v is the total cross-sectional area of fin base, A_c is the cross-sectional area of fin, and n is the number of fins. The surface area of one non-perforated fin has been derived as follows: -

$$A_f = 2W \times L_c + 2t \times L_c + t \times W \quad (14)$$

$$A_f = 2L_c(W + t) + t \times W \quad (15)$$

$$A_f = P_e L_c + A_c \quad (16)$$

Where; W, t, L_c, P_e are the fin width, thickness, characteristics length, and fin periphery respectively, which can be represented as:

$$L_c = L + \frac{t}{2} \quad (17)$$

$$p_e = 2(w + t) \quad (18)$$

The surface area of each perforation shape can be derived as shown below:-

For the rectangular perforations:

$$A_f = 2(W \times L_c - n_p \times a \times b) + 2t \times L_c + t \times W \quad (19)$$

$$A_f = 2L_c(W + t) - 2n_p \times a \times b + t \times W \quad (20)$$

$$A_f = P_e L_c - 2n_p \times a \times b + A_c \quad (21)$$

Where; n_p is the rectangular perforation number, a is the rectangular perforation height, and b is the rectangular perforation width.

For circular perforations:

$$A_f = P_e L_c - 2n_p \times \pi r^2 + A_c \quad (22)$$

Where; n_p is the circular perforation number, r is the circular perforation radius.

For V-perforations:

$$A_f = P_e L_c - 2n_p \times A_p + A_c \quad (23)$$

Where; n_p is the V-perforation number, $A_p$is the cross sectional area of the V-perforation.

The fin total surface area can be represented as:

$$A_t = n \times A_f + A_b \quad (24)$$

3.4. Average Heat Transfer Coefficient:

After calculating logarithmic mean temperature and total surface area as shown in equations (12) and (24), the coefficient of heat transfer can be calculated as follows:

$$h_{avg} = \frac{Q}{A_t \times T_m} \quad (25)$$

Where, Q is the input heat supplied.

3.5. Calculation of Nusselt number:

Nusselt number presents the affecting of the heat transfer by the difference in the surface area and disturbances in the flow because of fins. Thus it can be given in the following equation:

$$Nu = \frac{h_{avg} \times D_h}{k_{air}} \quad (26)$$

Where, D_h is the wind tunnel hydraulic diameter, and k_{air} is the air thermal conductivity.

3.6. Calculation of Reynolds number:

The convection from laminar flow to turbulent flow depends on the flow velocity, surface geometry, surface roughness, variety of fluid, and surface temperature, moreover, the ratio called Reynolds number, is a dimensionless quantity that represents the ratio of the inertia force to the viscous force of the working fluid flow:

$$Re = \frac{\rho_{air} \times V_{air} \times D_h}{\mu_{air}} \quad (27)$$

Where, ρ_{air} is the density of air, V_{air} velocity of air, and μ_{air} is the air dynamic viscosity that could be calculated from the previous equations (1) to (4).

3.7. Calculation of Friction losses:

To calculate the friction loss created with each fin perforation shape, two holes have been drilled on the back wall of the wind tunnel in order to measure pressure drop across the test length. An inclined manometer has been used for measuring the pressure drop using alcohol of 790 kg/m^3 density. Energy balance was made in order to find friction loss which is expressed as follows [10]:

$$f = \frac{\left(\frac{\Delta p}{\rho g} - \Delta z\right)}{4\left(\frac{L_t}{D_h} \cdot \frac{V^2}{2g}\right)} \quad (28)$$

Since the wind tunnel is vertical, the height difference in Z-direction has been taken into consideration.

4. RESULTS AND DISCUSSION:

4.1. Temperature distribution difference:

The trials have been done on steady-state circumstances as mentioned in section (2.3). The results ought to show a lower declivity of overall temperature for forced convection, showing that forced convection gives a good spread of temperature along the extended surfaces, making them work more efficiently as shown in Figure (10), which illustrates the difference in temperature along the length of the fin. If the extended surfaces were manufactured from an ideal conductor, it would be near highly efficient

surfaces and the gradient would be near horizontal.

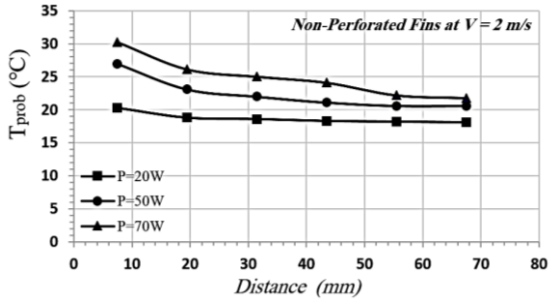

(a)

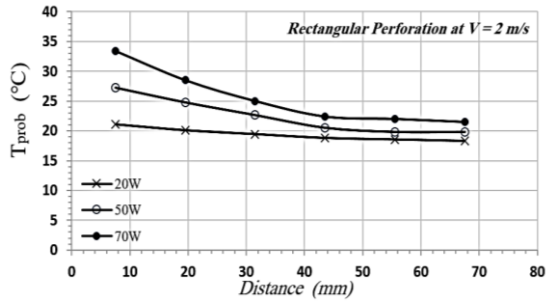

(b)

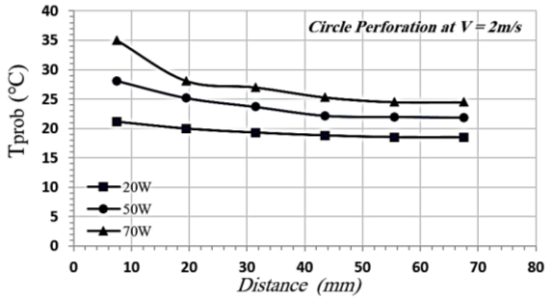

(c)

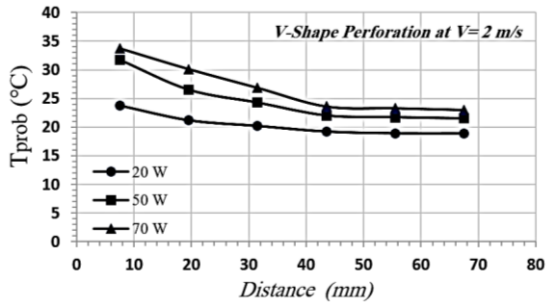

(d)

Figure (10): Temperature distribution along the Brass finned surfaces of non-perforated and different perforation shapes for three input powers, at V = 2 m/s.

Figure (10) shows the changes in temperature difference at a velocity of (2 m/s), which is relatively low, so that it is difficult to notice the changes in the temperature, which leads to the neglect of changes in Reynolds number and Nusselt number, hence the idea of research in low speeds. For more accuracy, Figure (11) represents a comparison between the different shapes perforation and the non-perforated one for low velocity (2 m/s) and for a chosen input power of (50 W).

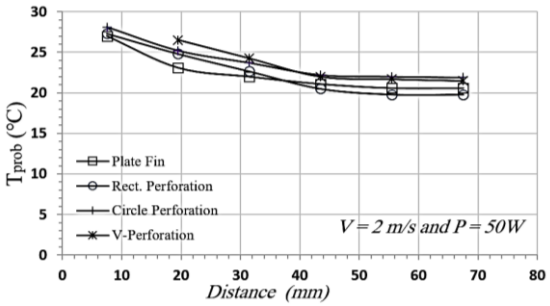

Figure (11): Comparison between the different shapes perforation and the non-perforated one for low velocity (2 m/s) and for a chosen input power of (50 W).

It is observed from Figure (11) of perforated fins that there is a decrease in the temperature at different locations along the fin length compared to the same case when no rectangular or circular or V-shape perforation was done. But after sometime, the perforated fins as we increase the fan velocity, we observe a small increment in temperature as the fin pitch increases. As a comparison between the different shapes, it is observed that the non-perforated fin has lower temperature difference than the other perforations. Also, the rectangular and circular perforations are too close to each other in temperature difference, then the highest temperature difference was the V-shape perforation. The previous results will surely affect the heat transfer coefficient that will be discussed in detail.

4.2. Convective Heat Transfer Coefficient:

Figure (12) shows that the thermal resistance is typically defined as the temperature difference between the base temperature of the heat sink at the outlet and the bulk mean temperature of the fluid at the input per unit heat flow rate. Therefore, as velocity increases, the coefficient of heat transfer (h) rises, rising the cooling impact throughout the fin array. [11].

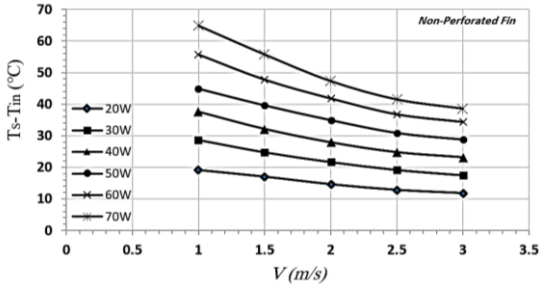

(a)

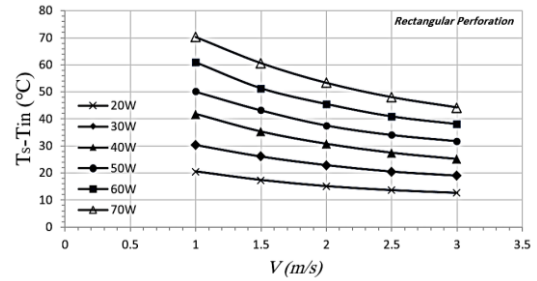

(b)

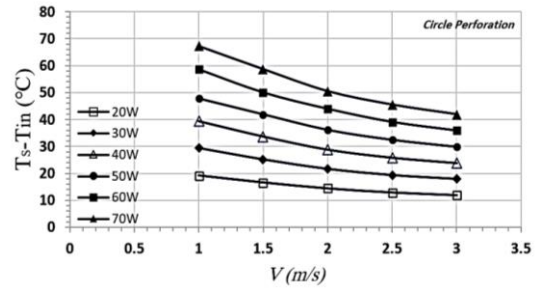

(c)

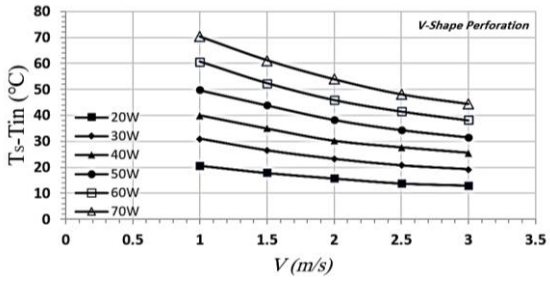

(d)

Figure (12): Temperature variation as a function of velocity for various input power voltages: (a) Non-perforated. (b) Rectangular Perforation. (c) Circular perforation, and (d) V-shape perforation.

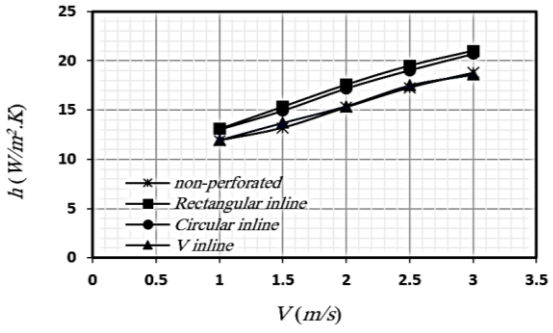

(a)

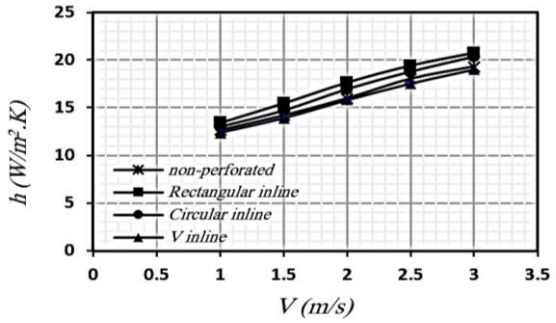

(b)

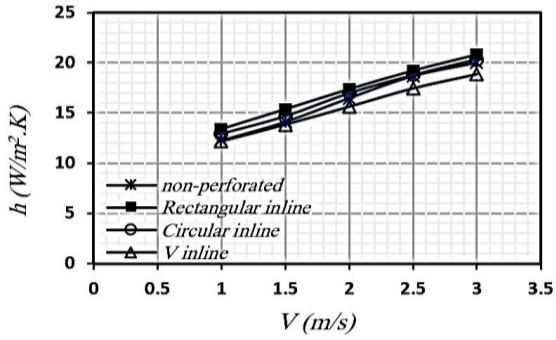

(c)

Figure (13): Heat transfer coefficient as a function of the velocity for selected input powers: (a) 20W. (b) 50W. (c) 70W

According to Figure (13), it can be noticed that the heat transfer coefficient of the non-perforated brass fins is minimum compared with the other perforations. The rectangular perforation is the highest values then the circular perforations, and the V-shape is approximately the same as non-perforated fins. This can be attributed to that the rectangular perforation has a larger shape, then the circular holes, and so on. This fact is due to that larger holes yield to increase the heat transfer rate, and that is because of increasing the heat transfer total surface area until it reaches its maximum rate, and that should be studied in detail in the future. Additionally, the perforation slows down the boundary layer's formation near the fin's surface, increasing the heat transfer rate. In other words, the airflow along the perforated fins is hampered by the presence of perforation. The flow disturbance causes flow separation, which results in increased turbulence and a faster rate of heat transfer. As a result, there are more holes, more flow separation happens, and turbulence mixing gets stronger.

4.3. Validation of experimental results for subdued input power:

The projected Nusselt number has a mean uncertainty of ±7%. The effect of change in the surface area, as well as that of disturbances in the flow as a result of the fins' effect on the augmentation of heat transfer, is represented by

the Nusselt number for the surface with fins calculated on the basis of projected area. However, Nusselt Figure suggested that the overall surface area merely reflected the impact of flow disruptions. Figure (14) shows the experimental Nusselt number fluctuation for fins with and without various geometries of perforation dependent on the total surface area and Reynolds number.

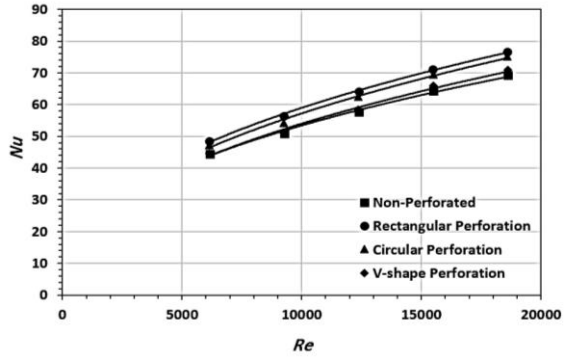

Figure (14): Experimental variation of Nusselt number based on the total surface area with Reynolds number for the fins with and without perforations.

The correlations that have been differentiated from the experimental results can be illustrated as:

a- Fins without perforation:

$$Nu = 1.274.(Re)^{0.4} \quad (29)$$

With the average friction factor:

$$f = 9369.(Re)^{-1.576} \quad (30)$$

b- Fins with Rectangular perforation:

$$Nu = 1.259.(Re)^{0.418} \quad (31)$$

With the average friction factor:

$$f = 387434.(Re)^{-1.86} \quad (32)$$

c- Fins with Circular perforation:

$$Nu = 1.1025.(Re)^{0.429} \quad (33)$$

With the average friction factor:

$$f = 228709.(Re)^{-1.839} \quad (34)$$

d- Fins with V-shape perforation:

$$Nu = 1.0556.(Re)^{0.427} \quad (35)$$

With the average friction factor:

$$f = 97478.(Re)^{-1.782} \quad (36)$$

The experimental average Nusselt number against a differentiated one was undertaken in the current study, and it was compared with earlier research while taking the boundary circumstances of those earlier studies' applications into account. Figure (15) compares the current and published correlations with an empirical equation that is differentiated based on the average of all correlations without perforations and is approximated using least squares.

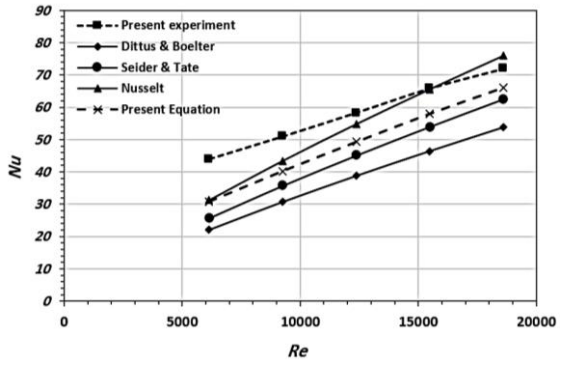

Figure (15): Experimental and differentiated correlations compared with the published works.

The conducted equation can be illustrated as follows:

$$Nu = 0.0744.(Re)^{0.69}.(Pr)^{0.2} \quad (37)$$

The equation is valid for Reynolds and Prandtl numbers range:

$$6000 \leq Re \leq 19000 \ and \quad \Pr \cong 0.7$$
$$with\ input\ power \quad 20\,W \leq P \leq 70\,W$$

Which could be applicable with regression coefficient $R^2 = 0.994$.

4.4. Friction Factor:

The friction factor was calculated from the measured values of pressure drop across the working test length L_t = *50 cm*. Figure (16) illustrate the friction factor variation with Reynolds number for different shapes perforation of the fin array. The in-line rectangular, circular and V-shape perforation arrays cause a significant pressure drop compared with the non-perforated smooth fin surface. As expected that resistance to flow is smaller due to the in-line array, and the friction factor was low in spite of the enhancement in the coefficient of heat transfer, so it is possible to evaluate the net energy gain due to the fins.

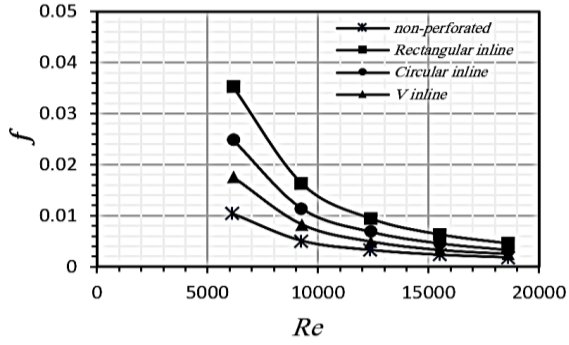

Figure (16): Variation of friction factor with Reynolds number for different perforation shapes.

A major aspect of determining the strength of an external force, like a fan, is friction. In reality, the running costs will increase if the friction factor increases since a stronger fan and more energy are required. Figure (16) illustrates how these new forms of perforated fins are less expensive to operate than solid fins when using an external convective force like a fan.

4.5. Fin Efficiency:

Fin efficiency can be defined as the ratio of the actual heat transferred to the heat that would be transferred if the entire fin area were at base temperature (or maximum heat transferred) [9]. Figure (17) represents the variation of the thermal efficiency as a function of the Reynolds number for selected input powers.

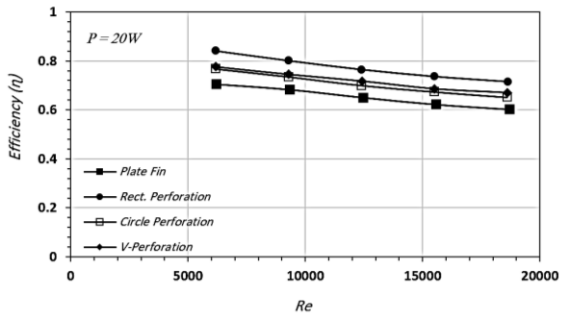

(a)

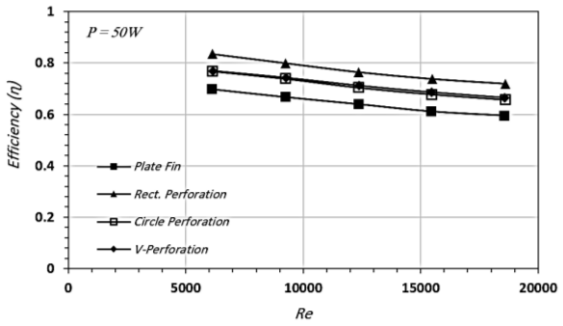

(b)

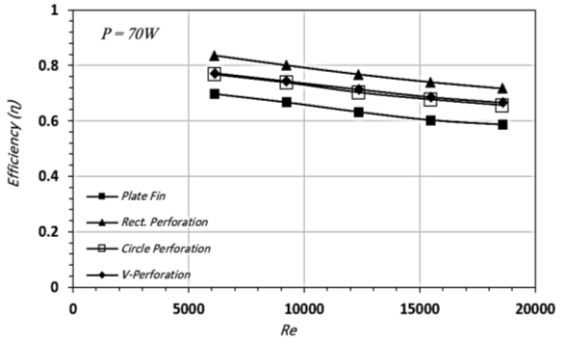

(c)

Figure (17): Thermal efficiency as a function of Reynolds number for selected input powers: (a) 20W. (b) 50W. (c) 70W

Figure (17) demonstrates that solid plate fins are less efficient than perforated plate fins. This is because the friction factor in Figure (16) represents the pressure drop for perforated plate fins as being lower than that for solid plate fins. Because convective heat transfer increases with velocity, the average Nusselt number for the experiment also rises as the Reynolds number does. As a result of the larger Nusselt number, perforated plate fins had more thermal efficiency than solid plate fins; nevertheless, as the Reynolds number increased, the friction factor decreased, lowering the heat sink's thermal efficiency.

5. CONCLUSION

Experimental research is done on the thermal properties of heat sinks with perforated and non-perforated plate fins. In general, the current effort is mainly focused on improving the thermal performance of the non-perforated plate fins and researching the impact of perforation and its shape on heat sink fins. The findings can be distilled into the following:

1. It was observed that the heat transfer coefficient increased with increasing flow velocity As a result, Nusselt number increased with increasing the Reynolds number. Where increasing Reynolds number will decrease the boundary layer that yield to enhancement in heat transfer.
2. The heat transfer from a surface equipped with flat non-perforated fins was investigated. The rectangular perforation of the fins gave higher enhancement than the circular and V-shape perforation, where the circular and V-shape perforation of the fins are approximately near each other in thermal performance, and all perforations show higher enhancement than the non-perforated fins.
3. As a consequence of the heat transfer improvement, the friction factor was higher for the rectangular and circular perforation than the V-shape and non-perforated fins. Therefore, it reduces the pumping power.
4. As a result, the fins efficiency of the rectangular perforation is higher than the others, then the circular and V-shape are close to each other. This illustrates the enhancement of heat transfer from the total fins surfaces of the perforation than the non-perforated fins.
5. Experimental correlations have been conducted depending on the experimental results that can be used within uncertainty ±7% for Brass materials used in the study.
6. Based on the experimental average, Nusselt number performed against a differentiated one and compared with previous works published while taking the boundary circumstances of

their application into account to synchronize with the current study, general correlations have been established for non-perforated fins. The correlation indicates a good level of agreement with the earlier works.

ACKNOWLEDGEMENTS

Researchers would like to thank the Department of Mechanical Engineering at the University of Duhok for allocating heat transfer lab facilities while conducting experimental tests.

NOMENCLATURE

a	Perforated fin height (m)
A_b	Surface area of fin base without fins (m^2)
A_c	Cross-sectional area of fin (m^2)
A_f	Surface area of one non-perforated fin (m^2)
A_p	Cross-sectional area of V-shape perforated fin (m^2)
A_v	Total cross-sectional area of fin base (m^2)
b	Perforated fin width (m)
C_p	Thermal heat capacity (kJ/kg.^{o}C)
D_h	Wind tunnel hydraulic diameter (m)
f	Friction factor
g	Gravitational acceleration (m/sec^2)
h	Heat transfer coefficient ($W/m^2.K$)
k	Thermal conductivity (W/m.^{o}C)
L	Fin length (m)
L_c	Fin characteristic length (m)
$LMTD$	Logarithmic Mean Temperature Difference (^{o}C)
n	Number of fins
Nu	Nusselt number
P_e	Fin periphery (m)
Pr	Prandtl number
Q	Input Heat supplied (W)
$\dot{Q_{cond}}$	Conduction heat transfer rate (W)
$\dot{Q_{conv}}$	Convection heat transfer rate (W)
$\dot{Q_{rad}}$	Radiation heat transfer rate (W)
Q_f	Fin heat transfer (W)
Q_{nf}	Heat transfer without fins (W)
r	Circular perforation radius (m)
Re	Reynolds number
t	Fin thickness (m)
T_{avg}	Average air mean temperature (^{o}C)
T_{in}	Inlet air temperature (^{o}C)
T_m	LMTD
T_{out}	Outlet air temperature (^{o}C)
T_s	Fin base surface temperature (^{o}C)
V	Velocity (m/sec)
w	Fin width (m)

Greek letters

ΔP	Pressure drop (*Pascal*)
ρ	Density (kg/m^3)
μ	Dynamic viscosity (kg/m.s)
η	Fin efficieny

REFERENCES

[1] O. Sara, T. Pekdemir, S. Yapici, and M. Yilmaz, "Heat-transfer enhancement in a channel flow with perforated rectangular blocks," *International Journal of Heat and Fluid Flow*, vol. 22, no. 5, pp. 509–518, 2001.

[2] U. Akyol and K. Bilen, "Heat transfer and thermal performance analysis of a surface with hollow rectangular fins," *Applied Thermal Engineering*, vol. 26, no. 2–3, pp. 209–216, 2006.

[3] K. H., "Thermal Analysis of Square and Circular Perforated Fin Arrays by Forced Convection," *International Journal of Current Engineering and Technology*, vol. 2, pp. 109–114, Jan. 2013, doi: 10.14741/ijcet/spl.2.2014.20.

[4] T. K. Ibrahim *et al.*, "Experimental study on the effect of perforations shapes on vertical heated fins performance under forced convection heat transfer," *International Journal of Heat and Mass Transfer*, vol. 118, pp. 832–846, 2018.

[5] M. Mohammad, M. P. H. Talukder, K. A. Rahman, and M. W. Hridoy, "Experimental Investigation on the Effect of Different Perforation Geometry of Vertical Fins Under Forced Convection Heat Transfer," in *International Conference on Mechanical Engineering and Renewable Energy*, 11-13 Dec 2019.

[6] R. Adhikari, D. Wood, and M. Pahlevani, "An experimental and numerical study of forced convection heat transfer from rectangular fins at low Reynolds numbers," *International Journal of Heat and Mass Transfer*, vol. 163, p. 120418, 2020.

[7] T. K. Ibrahim, A. T. Al-Sammarraie, M. S. Al-Jethelah, W. H. Al-Doori, M. R. Salimpour, and H. Tao, "The impact of square shape perforations on the enhanced heat transfer from fins: Experimental and numerical study," *International Journal of Thermal Sciences*, vol. 149, p. 106144, 2020.

[8] A. R. Kaladgi *et al.*, "Heat transfer enhancement of rectangular fins with circular perforations," *Materials Today: Proceedings*, vol. 47, pp. 6185–6191, 2021.

[9] J. P. Holman, *Heat transfer*, 10th edition, McGraw-Hill, 2010.

[10] J. F. Douglas, J. M. Gasiorex, J. A. Swaffield, and L. B. Jack, *Fluid Mechanics*, 5th edition, Prentice Hall, 2005.

[11] A. F. SAEED and O. A. ABBO, "Design, and Manufacturing a Small-scale Wind Tunnel for Heat Transfer Analysis of Flat Plate and Finned Plate Heat Sinks," *Journal of Duhok University*, vol. 23, no. 2, pp. 693–706, 2020.

التأثير التجريبي لتحسين انتقال الحرارة بالحمل القسري من مصفوفة زعانف مثقبة

نوري رعد نوري*
noorikhlka34@gmail.com

اركان فوزي سعيد**
arkan.alhazeen@uod.ac

* جامعة دهوك بوليتكنيك - الكلية التقنية للهندسة - قسم هندسة الطاقة -دهوك -العراق
** جامعة دهوك - كلية الهندسة – قسم الهندسة الميكانيكية - دهوك - العراق

تاريخ الاستلام:19-10-2022 استلم بصيغته المنقحة: 22-11-2022 تاريخ القبول:4-12-2022

الملخص

تم اختبار انتقال الحرارة بالحمل القسري عملياً من سطح زعانف مستطيلة مثبتة على سطح شاقولي لعدد رينولدز واطئ. تم تقييس انتقال الحرارة لعدد من الزعانف المثقبة وغير المثقبة، مسافة الزعانف، والطول في جريان هواء صاعد متغير السرعة مع طاقة حرارية منخفضة ضمن حدود 20 واط و 70واط. تم فحص الخصائص لمصفوفة زعنفة مثقبة مستطيلة ودائرية وعلى شكل V *مقابل مصفوفة غير مثقبة. تم دراسة تأثير الشروط الحدية المختلفة، مثل الحرارة الداخلة مع تغير سرعة الهواء على متوسط معامل نقل الحرارة (*h*). تم فحص تأثير رقم (*Nu*) و رقم (*Re*) عملياً. لوحظ تحسن بالحرارة المفقودة عن طريق زيادة معامل انتقال الحرارة بين سطح الزعنفة الكلي والظروف المحيطة به، عن طريق زيادة مساحة انتقال الحرارة وإزالة جزء من السطح الخارجي من خلال تثقيب الزعانف. تم استنتاج علاقات تجريبية تربط رقمي* Nu *و* Re *للمشتت الحراري للوحة غير المثقبة والوصول إلى* $6*10^3 \le Re \le 19*10^3$ *وعدد برانتل* $Pr \cong 0.7$ *مع نسبة خطأ* ± 7 *٪ ، وللمشتت الحراري ذات الزعانف المثقبة والوصول إلى* $6*10^3 \le Re \le 20*10^3$ *و* $Pr \cong 0.7$ *مع عامل الانحراف* R^2 = 0.995. *تم قياس عامل الاحتكاك أيضًا من خلال قياس انخفاض الضغط على طول مقطع الاختبار في النفق الهوائي وتم استنتاج الفرق بين الصفائح المختلفة.*

الكلمات الداله :

انتقال الحرارة بالحمل القسري، تحسين الانتقال الحراري، السطوح الممتدة المثقبة.